Hybrid Optimization Method for High-performance Cascade Structure Feedback Controller Design

Yoshihiro Maeda
Department of Electrical and Mechanical Engineering
Nagoya Institute of Technology
Gokiso, Showa, Nagoya 4668555, JAPAN
Email: ymaeda@nitech.ac.jp

Eitaro Kuroda
Department of Electrical and Mechanical Engineering
Nagoya Institute of Technology
Gokiso, Showa, Nagoya 4668555, JAPAN
Email: e.kuroda.963@stn.nitech.ac.jp

Takahiro Uchizono
Department of Electrical and Mechanical Engineering
Nagoya Institute of Technology
Gokiso, Showa, Nagoya 4668555, JAPAN
Email: t.uchizono.358@stn.nitech.ac.jp

Makoto Iwasaki
Department of Electrical and Mechanical Engineering
Nagoya Institute of Technology
Gokiso, Showa, Nagoya 4668555, JAPAN
Email: iwasaki@nitech.ac.jp

Abstract—**This paper presents an efficient hybrid optimization method to design a high-performance cascade structure feedback (FB) controller for a mechatronic system with resonant vibration modes. The proposed method combines sequential quadratic programming and a genetic algorithm (GA) in order to obtain the parameters of the cascade structure FB controller. The proposed method makes it possible to obtain a wide-bandwidth FB controller that satisfies the specified stability margins and sensitibity function gains for resonant modes in a short design time. This paper describes the hybrid optimization method and design procedure for the cascade structure FB controller in detail. In addition, it shows how the effectiveness of the proposed method was evaluated through frequency-domain simulations using a laboratory galvano scanner, in comparison with the conventional GA-based optimization method.**

I. Introduction

The design of a wide-bandwidth feedback (FB) controller is one of the important indices for the fast-response and high-precision motion control of mechatronic systems. In particular, for plant systems that include high-order resonant vibration modes, it is well-known that designing a fine FB controller is a difficult and complicated problem [1], [2]. Although gain/phase stabilization [3] is a highly effective approach to expand the control bandwidth, the design procedure is still complex, and great skill is required of industrial engineers. In the gain/phase stabilization approach, the FB controller is generally defined as a *cascade structure* controller connecting a PID (or phase lead/lag) compensator and some resonant mode compensators in series, where each structural compensator has parameters that need to be designed [3], [4].

In recent years, numerical optimization-based FB controller design approaches such as convex optimization (LMIs) [4]−[7] and nonlinear programming [8], [9] have aggressively been studied in the related research fields in order to obtain a wide-bandwidth FB controller with less labor. However, since the parameters have nonlinear relationships with each other in a *cascade structure* controller, which generaly makes it difficult to find global optimum parameters, a numerical optimization-based approach can only be used to design specific parameters for a portion of the controller. Therefore, the other parameters need to be manually given in advance [5], [8], which becomes another complex problem in the controller design. Although meta-heuristic optimization methods such as a genetic algorithm (GA) are promising approaches to directly design all of the parameters, it is well-known that the searching time tends to be long when the design problem is difficult.

This paper presents a hybrid optimization method [10] that combines sequential quadratic programing (SQP) and a GA in order to efficiently design a wide-bandwidth *cascade structure* FB controller for a resonant system. In the proposed method, the SQP-based optimization efficiently obtains parameters for the numerator of a PID compensator, based on a constrained optimization problem, which pursues the control bandwidth and ensures the specified system stability (gain and phase margins) and sensitivity function gains for the resonant modes. On the other hand, the GA-based optimization achieves the other parameters in the PID and resonant mode compensators. By applying the proposed method, a wide-bandwidth FB controller for a resonant system can be designed in a short time, compared with the conventional GA-based optimization method. The effectiveness of the proposed method was verified through frequency-domain simulations of a laboratory galvano scanner as an example resonant system.

II. Design Problem

The design of a single-input-single-output FB controller for the typical FB control system shown in Fig. 1 was considered in this study. In the FB control system, $C(s)$ is the FB controller, $P(s)$ is the plant, r is the reference for the system input, y is the control output as the system output, and u is the control input. $C(s)$ is defined as a cascade structure controller as follows, by connecting a PID compensator $C_{PID}(s)$ and
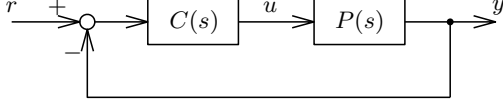
Fig. 1. Block diagram of FB control system.

N_R-pieces second-order resonant mode compensators $C_{Ri}(s)$ in series ($N_R \in \mathbb{N}$):

$$C(s) = C_{PID}(s) \prod_{i=1}^{N_R} C_{Ri}(s), \qquad (1)$$

$$C_{PID}(s) = K_P + \frac{K_I}{s} + \frac{K_D s}{T_D s + 1}, \qquad (2)$$

$$C_{Ri}(s) = \frac{s^2 + 2\zeta_{Rni}\omega_{Ri}s + \omega_{Ri}^2}{s^2 + 2\zeta_{Rdi}\omega_{Ri}s + \omega_{Ri}^2}. \qquad (3)$$

The aim of $C_{Ri}(s)$ is to stabilize the resonant modes in $P(s)$ and sufficiently attenuate the vibratory responses, and it is well-known that the gain/phase stabilization approach [3], [4] can effectively expand the control bandwidth.

The design problem of $C(s)$ is to obtain all of the controller parameters defined by (4) that can expand the control bandwidth as much as possible while satisfying the specified gain margin of g_m dB and phase margin of ϕ_m deg.

$$\eta_C = \{K_P, K_I, K_D, T_D, \omega_{R1}, \zeta_{Rn1}, \zeta_{Rd1},$$
$$\ldots, \omega_{RN_R}, \zeta_{RnN_R}, \zeta_{RdN_R}\} \in \mathbb{R} \quad (4)$$

III. HYBRID OPTIMIZATION METHOD

A. Reformulation of FB Controller

In order to design η_C using the hybrid optimization method, $C_{PID}(s)$ of (2) is reformulated as (5) with undetermined PID parameter vector $\boldsymbol{\rho}_{PID} \in \mathbb{R}^{3\times 1}$.

$$C_{PID}(s) = \boldsymbol{\Psi}_{PID}(s)\boldsymbol{\rho}_{PID} \qquad (5)$$

$$\boldsymbol{\Psi}_{PID}(s) = \begin{bmatrix} 1 & \dfrac{1}{s} & \dfrac{s}{T_D s + 1} \end{bmatrix}$$

$$\boldsymbol{\rho}_{PID} = \begin{bmatrix} K_P & K_I & K_D \end{bmatrix}^T$$

By using (5), (1) can be expressed as follows:

$$C(s) = \prod_{i=1}^{N_R} C_{Ri}(s)\boldsymbol{\Psi}_{PID}(s)\boldsymbol{\rho}_{PID} = \boldsymbol{\Psi}_C(s)\boldsymbol{\rho}_{PID}. \qquad (6)$$

Note that $C(s)$ becomes an affine function for $\boldsymbol{\rho}_{PID}$. Therefore, η_C to be designed can be expressed as (7), by separating it into the PID parameters η_{PID} and the other parameters η_{oth}.

$$\eta_C = \{\eta_{PID}, \eta_{oth}\}, \qquad (7)$$
$$\eta_{PID} = \{K_P, K_I, K_D\},$$
$$\eta_{oth} = \{T_D, \omega_{R1}, \zeta_{Rn1}, \zeta_{Rd1}, \ldots, \omega_{RN_R}, \zeta_{RnN_R}, \zeta_{RdN_R}\}$$
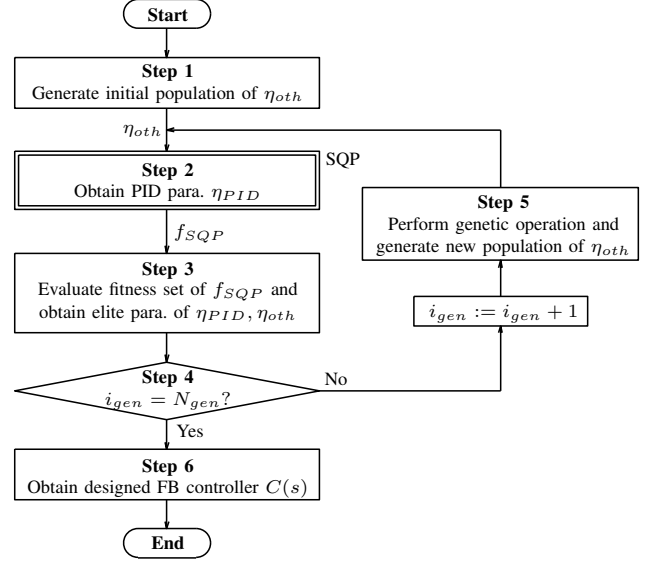
Fig. 2. Flowchart of hybrid optimization method using SQP and GA.

B. Design Procedure

A flowchart for the proposed hybrid optimization-based FB controller design method is shown in Fig. 2. The proposed method combines two optimization algorithms (SQP and GA) to obtain the parameters for the cascade structure FB controller such as (1). The SQP-based optimization obtains the PID parameters η_{PID} using the SQP's efficient searching ability. On the other hand, the GA-based optimization finds the other parameters η_{oth}, which cannot be directly handled by convex optimization or easily solved by nonlinear programming methods [5]−[7], using the meta-heuristic approach [10]. The detailed design procedure is as follows.

- **Step 1:** The GA randomly generates the initial population of η_{oth} (a population has N_{ind} individuals) as the first generation ($i_{gen} = 1$).
- **Step 2:** Appropriate PID parameters η_{PID} ($\boldsymbol{\rho}_{PID}$) for N_{ind} candidates of η_{oth} are obtained by the SQP-based optimization, which minimizes the objective function $\mathcal{J}_{SQP}$ under the specified constraints. The fitness scores f_{SQP} of the SQP are transferred to step 3.
- **Step 3:** All of the fitness scores f_{SQP} are evaluated in the GA, and the elite parameters η_{PID} and η_{oth} of the elite individual are obtained.
- **Step 4:** If generation i_{gen} is less than the specified number N_{gen}, then $i_{gen} := i_{gen} + 1$ and go to step 5; else, go to step 6.
- **Step 5:** Genetic operations such as selection, crossover, and mutation are performed, and a new population of η_{oth} for the next generation is generated. While $i_{gen} \leq N_{gen}$, steps $2 \sim 5$ are repeated.
- **Step 6:** The desired $C(s)$ is obtained with the elite η_{PID} and η_{oth}, which can expand the control bandwidth while satisfying the specified stability margins and sensitivity gains for the resonant modes.
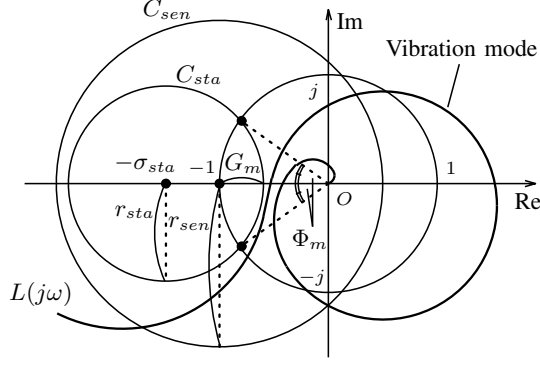
Fig. 3. Circle condition for Nyquist trajectory.

C. SQP-based Parameter Optimization

1) Objective Function for Expanding Control Bandwidth:
The objective function $\mathcal{J}_{SQP}$, which is prepared to expand the control bandwidth, is introduced in the design of PID parameters η_{PID} ($\boldsymbol{\rho}_{PID}$). First, the desired frequency-domain sensitivity function $S_{des}(j\omega)$ is manually defined to specify the target control bandwidth. Then, the desired frequency response function of the open-loop $L_{des}(j\omega)$ is formulated as (8) using $S_{des}(j\omega)$.

$$L_{des}(j\omega) = \frac{1 - S_{des}(j\omega)}{S_{des}(j\omega)} \tag{8}$$

Here, the distance $e_L(\omega)$ between the desired open-loop $L_{des}(j\omega)$ and the actual open-loop $L(j\omega) = C(j\omega)P(j\omega)$ at a frequency ω on the complex plane can be expressed as follows:

$$e_L(\omega) = |L_{des}(j\omega) - L(j\omega)| = \left| \boldsymbol{Y}_L(j\omega) \begin{bmatrix} 1 \\ \boldsymbol{\rho}_{PID} \end{bmatrix} \right|, \tag{9}$$

$$\boldsymbol{Y}_L(j\omega) = \begin{bmatrix} L_{des}(j\omega) & -P(j\omega)\boldsymbol{\Psi}_C(j\omega) \end{bmatrix}$$
$$= \begin{bmatrix} L_{des}(j\omega) & -\boldsymbol{\Psi}_L(j\omega) \end{bmatrix} \in \mathbb{C}^{1\times 4}.$$

By using (9), $\mathcal{J}_{SQP}$ is defined by (10) as the summation of the squared $e_L(\omega)$ at the discrete-frequencies $\Omega_k (k = 1, \ldots, N_k)$:

$$\mathcal{J}_{SQP} = \sum_{k=1}^{N_k} e_L(\Omega_k)^2$$
$$= \begin{bmatrix} 1 & \boldsymbol{\rho}_{PID}^T \end{bmatrix} \boldsymbol{Y}_L(j\Omega_k)^T \boldsymbol{Y}_L(j\Omega_k) \begin{bmatrix} 1 \\ \boldsymbol{\rho}_{PID} \end{bmatrix}. \tag{10}$$

In general, Ω_k is selected at low frequencies below the target control bandwidth.

2) Constraint for System Stability: Both the gain margin and phase margin are ensured by using inequality constraints with respect to $\boldsymbol{\rho}_{PID}$, on the basis of the circle condition method for a Nyquist diagram [6], [8]. Fig. 3 shows a conceptual diagram of the circle condition, where the bold line is an example Nyquist trajectory of the open-loop $L(j\omega)$, and C_{sta} is the specified circle with a center at $(-\sigma_{sta}, j0)$ and a radius of r_{sta} for stating the stability margins. The distance between the Nyquist point $(-1, j0)$ and the intersection of

C_{sta} on the real axis represents the gain margin G_m ($g_m = 20\log_{10} G_m$ [dB]), while the angle between two intersections of C_{sta} and the unit circle represents the phase margin Φ_m ($\phi_m = 180\Phi_m/\pi$ [deg]). The circle condition for the stability margins is mathematically formulated by (11), which means the Nyquist trajectory passes the outside of C_{sta} at a frequency ω.

$$|L(j\omega) + \sigma_{sta}| > r_{sta}, \tag{11}$$
$$\sigma_{sta} = \frac{G_m^2 - 1}{2G_m(G_m\cos\Phi_m - 1)},$$
$$r_{sta} = \frac{(G_m - 1)^2 + 2G_m(1 - \cos\Phi_m)}{2G_m(G_m\cos\Phi_m - 1)}$$

Here, in order to achieve a stable FB control system, the following conditions should be satisfied.

$$0 < r_{sta} < \sigma_{sta}, \quad (\sigma_{sta} - 1)^2 < r_{sta}^2 \tag{12}$$

By considering (5), (11) is reformulated as follows:

$$|\boldsymbol{\Psi}_L(j\omega)\boldsymbol{\rho}_{PID} + \sigma_{sta}| = \left| \boldsymbol{Y}_{sta}(j\omega) \begin{bmatrix} 1 \\ \boldsymbol{\rho}_{PID} \end{bmatrix} \right| > r_{sta}, \tag{13}$$
$$\boldsymbol{Y}_{sta} = \begin{bmatrix} \sigma_{sta} & \boldsymbol{\Psi}_L(j\omega) \end{bmatrix} \in \mathbb{C}^{1\times 4}.$$

By squaring and reformulating (13), the inequality constraint for the stability margins can be defined by (14) as a function of $\boldsymbol{\rho}_{PID}$.

$$\mathcal{R}_{sta}(\omega) = \begin{bmatrix} 1 & \boldsymbol{\rho}_{PID}^T \end{bmatrix} \boldsymbol{Y}_{sta}(j\omega)^T \boldsymbol{Y}_{sta}(j\omega) \begin{bmatrix} 1 \\ \boldsymbol{\rho}_{PID} \end{bmatrix}$$
$$-r_{sta}^2 > 0. \tag{14}$$

3) Constraint for Sensitivity gain of Resonant Mode:
An additional circle condition for the resonant modes is introduced in order to sufficiently attenuate the sensitivity of the resonant modes that require compensation. The amplitude of the sensitivity at a frequency ω is represented by

$$|S(j\omega)| = \left| \frac{1}{1 + L(j\omega)} \right|. \tag{15}$$

Note that the denominator of the right hand side of (15) corresponds to the distance between the open-loop $L(j\omega)$ and the Nyquist point $(-1, j0)$. In order to attenuate $|S(j\omega)|$ less than the specified amplitude g_{sen} dB, i.e., $|S(j\omega)| < 10^{\frac{g_{sen}}{20}}$, the following inequality is defined:

$$|L(j\omega) + 1| > r_{sen}. \tag{16}$$

Inequality (16) implies that the Nyquist trajectory of $L(j\omega)$ should be described outside of the specified circle C_{sen} with a center at $(-1, j0)$ and a radius of $r_{sen} = 10^{-\frac{g_{sen}}{20}}$ in Fig. 3. Similar to section III-C2, (16) is transformed as follows:

$$|\boldsymbol{\Psi}_L(j\omega)\boldsymbol{\rho}_{PID} + 1| = \left| \boldsymbol{Y}_{sen}(j\omega) \begin{bmatrix} 1 \\ \boldsymbol{\rho}_{PID} \end{bmatrix} \right| > r_{sen}, \tag{17}$$
$$\boldsymbol{Y}_{sen} = \begin{bmatrix} 1 & \boldsymbol{\Psi}_L(j\omega) \end{bmatrix} \in \mathbb{C}^{1\times 4}.$$

Therefore, the inequality constraint for the sensitivity is
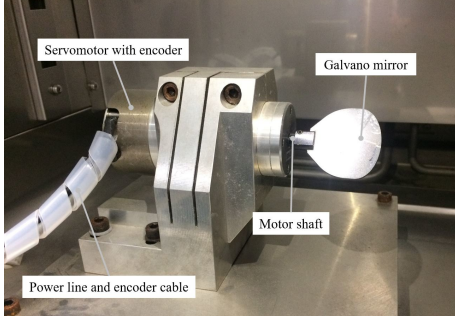
Fig. 4. Exterior of a laboratory galvano scanner.

Fig. 5. Bode plots of plant.

formulated by

$$\mathcal{R}_{sen}(\omega) = \begin{bmatrix} 1 & \boldsymbol{\rho}_{PID}^T \end{bmatrix} \mathbf{Y}_{sen}(j\omega)^T \mathbf{Y}_{sen}(j\omega) \begin{bmatrix} 1 \\ \boldsymbol{\rho}_{PID} \end{bmatrix} \\ -r_{sen}^2 > 0. \quad (18)$$

To achieve the desired sensitivity attenuation property, (18) is applied at specific frequencies around the resonant modes.

4) Optimization Problem: Finally, $\boldsymbol{\rho}_{PID}$ can be designed based on the following optimization problem, using $\mathcal{J}_{SQP}$ of (10), $\mathcal{R}_{sta}$ of (14), and $\mathcal{R}_{sen}$ of (18):

$$\min_{\boldsymbol{\rho}_{PID}} \quad \mathcal{J}_{SQP} \quad (19)$$
$$\text{subject to} \quad \mathcal{R}_{sta}(\Omega_p) > 0, \quad \mathcal{R}_{sen}(\Omega_q) > 0,$$

where $\Omega_p(p = 1, \ldots, N_p)$ and $\Omega_q(q = 1, \ldots, N_q)$ are the discrete frequencies where the inequality constraints are imposed. In this study, (19) is solved by SQP.

D. GA-based Parameter Optimization

In the GA-based optimization, the fitness f_{SQP} of (19) calculated by the SQP-based optimization is used as the fitness f_{GA} of the GA. In the genetic operation, simple methods (tournament selection, single-point crossover, and bit-string mutation) are utilized to ensure the simplicity and efficiency of the FB controller design.

IV. SIMULATION EXAMPLE

A. Target Plant

In this study, a laboratory galvano scanner for laser processing machines was used as the plant system. The external appearance of the laboratory galvano scanner is shown in Fig. 4. The galvano scanner is simply composed of a rotary motor, a mirror, and an optical encoder, and the fast-response and high-precision control of the motor angle is required to achieve a high production rate of high density interconnect (HDI) printed circuit boards. For details of the galvano scanner, see [10].

Fig. 5 shows the frequency characteristics of the galvano scanner (from the motor current reference i_{ref} to the detected motor angle θ_m), where the broken lines are the experimental results, and the solid lines are the plant model $P(j\omega)$. The model parameters were identified by using the nonlinear least
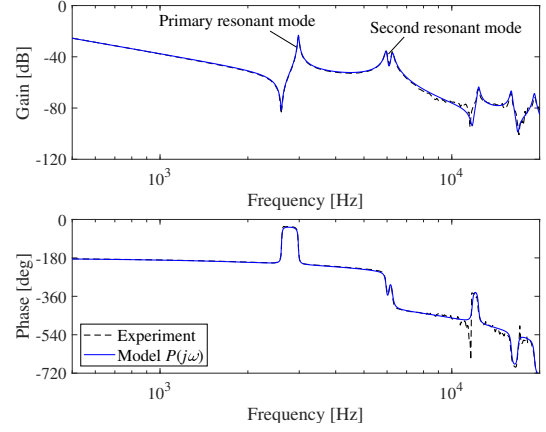
squares method. The galvano scanner has a primary resonant mode at 2980 Hz, a secondary resonant mode at 5965 Hz, other resonant modes in a frequency range greater than 10 kHz due to the mechanism, and a phase delay property due to the current control system and digital-to-analog (D/A) conversion at the controller. $P(s) = \theta_m(s)/i_{ref}(s)$ is formulated as (20) with consideration of the high-order resonant modes and the phase delay:

$$P(s) = e^{-Ls} K_p \left(\frac{1}{s^2} + \sum_{l=1}^{6} \frac{k_l}{s^2 + 2\zeta_l \omega_l s + \omega_l^2} \right), \quad (20)$$

where K_p is the gain (considering the moment of inertia, torque constant of the motor, and steady gain of the current controller), ω_l is the natural angular frequency, ζ_l is the damping coefficient, k_l is the resonant mode gain, and L is the equivalent dead time. In the following simulation evaluation, $P(s)$ of (20) is used as the plant in Fig. 1, and its frequency response function $P(j\omega)$ is adopted in the FB controller design.

B. Application of Proposed Method

The FB controller $C(s)$ was designed according to the proposed method presented in section III. In this study, $N_R = 2$ was selected to stabilize the primary and secondary resonant modes, since these two resonant modes significantly affect the system stability.

First, in order to define the circle condition $\mathcal{R}_{sta}$ of (14) specifing the gain and phase margins of $g_m = 5$ dB and $\phi_m = 30$ deg, the circle parameters σ_{sta} and r_{sta} were respectively assigned as $\sigma_{sm} = 1.13$ and $r_{sm} = 0.56$. The following applied frequencies Ω_p were selected: $\Omega_p = 2\pi \times 100 \sim 2\pi \times 25000$ rad/s $(N_p = 10000)$.

Second, two circle conditions $\mathcal{R}_{sen1}$ and $\mathcal{R}_{sen2}$ of (18) were respectively imposed for the sensitivity of the primary and secondary resonant modes. The boundaries g_{sen1} and g_{sen2} were set to $g_{sen1} = -20$ dB and $g_{sen2} = -10$ dB (i.e., $r_{sen1} = 10.00$ and $r_{sen3} = 3.16$), while the applied frequencies Ω_{1q} and Ω_{2q} were set to $\Omega_{1q} = 2\pi \times 2980$ rad/s $(N_{1q} = 1)$ and $\Omega_{2q} = 2\pi \times 5965$ rad/s $(N_{2q} = 1)$,

Generation number N_{gen}	10000
Individual number N_{ind}	10
Selection rate	1.0
Crossover rate	0.9
Mutation rate	0.05

TABLE II
PARAMETER SEARCH RANGE OF η_{oth} IN GA-BASED OPTIMIZATION.

Parameter	Minimum	Maximum
T_D [s^{-1}]	1.59×10^{-4}	0.59×10^{-4}
ω_{R1} [rad/s]	$2\pi \times 1000$	$2\pi \times 2960$
ζ_{Rn1}	-1	1
ζ_{Rd1}	0	1
ω_{R2} [rad/s]	$2\pi \times 5965$	$2\pi \times 12000$
ζ_{Rn2}	-1	1
ζ_{Rd2}	0	1

Fig. 6. Fitness for generation.

where each resonant mode had the highest gain, as shown in Fig. 5.

Third, the desired sensitivity function $S_{des}(j\omega)$ to expand the control bandwidth was simply assigned as (21) in the Laplace-domain expression, with consideration of the rigid mode of the plant and the integral compensation of the PID compensator in the low frequency range:

$$S_{des}(s) = \frac{K_S s^3}{(s + \omega_{S1})(s^2 + 2\zeta_{S2}\omega_{S2}s + \omega_{S2}^2)}, \quad (21)$$

where the parameters were respectively determined to be $K_S = 1.2$, $\omega_{S1} = 2\pi \times 700$ rad/s, $\omega_{S2} = 2\pi \times 800$ rad/s, and $\zeta_{S2} = 0.6$. This parameter setting was a strict condition for achieving a wider control bandwidth. $L_{des}(j\omega)$ to define the objective function $\mathcal{J}_{SQP}$ was calculated according to (8), while the evaluated frequencies were set as $\Omega_k = 2\pi \times 100 \sim 2\pi \times 1000$ rad/s ($N_k = 500$).

For the GA-based optimization, the parameters of the genetic operation were set as listed in Table I, while the search ranges of η_{oth} were chosen as listed in Table II.

C. Comparative Evaluation

The proposed hybrid optimization method was applied to the galvano scanner in order to verify the effectiveness of a high-performance FB controller design. For comparison, the conventional GA-based optimization method, which designs all of the parameters η_C using only the GA, was simultaneously evaluated. The objective function $\mathcal{J}_{GA}$ of the conventional method is defined as follows:

$$\mathcal{J}_{GA} = \sum_{k=1}^{N_k} e_L(\Omega_k)^2 + \mathcal{J}_{sta} + \mathcal{J}_{sen1} + \mathcal{J}_{sen2}, \quad (22)$$

$$\mathcal{J}_{sta} = \begin{cases} 0 & (|L(j\Omega_p) + \sigma_{sta}| > r_{sta}) \\ 10^{17} & (|L(j\Omega_p) + \sigma_{sta}| \leq r_{sta}) \end{cases},$$

$$\mathcal{J}_{sen1} = \begin{cases} 0 & (|L(j\Omega_{1q}) + 1| > r_{sen1}) \\ 10^{17} & (|L(j\Omega_{1q}) + 1| \leq r_{sen1}) \end{cases},$$

$$\mathcal{J}_{sen2} = \begin{cases} 0 & (|L(j\Omega_{2q}) + 1| > r_{sen2}) \\ 10^{17} & (|L(j\Omega_{2q}) + 1| \leq r_{sen2}) \end{cases}.$$

In (22), the first term on the right hand side is same as $\mathcal{J}_{SQP}$ of (10), while the second, third, and fourth terms are respectively penalty functions that become large values when the circle conditions on the stability margins and the sensitivity of the resonant modes are not satisfied.

Fig. 6 shows the comparative elite fitness of f_{GA} for generation N_{gen}, where both the proposed and conventional methods are performed three times. Note that the vertical axis shows log scale values (i.e., $\log_{10} f_{GA}$). In the conventional method, there was fluctuation of the convergence speed and final fitness, and it took at least 3 h to obtain the elite parameters in the case of the shortest design time. On the other hand, the proposed method could stably achieve the elite parameters in every trials, and the average design time was approximately 1 h that was less than one third of the shortest time of the conventional method.

Next, the frequency characteristics of the FB control system using the designed $C(s)$ (best elite cases) are shown in Fig. 7. Although the designed FB controllers had different frequency characteristics, especially around the primary and secondary resonant modes in Fig. 7(a), both methods successfully ensured the specified stability margins and sensitivity of the resonant modes in Figs. 7(c) and 7(d). Note that although the proposed method could design almost the same FB controllers by three times of trials, the conventional method could not do it. On the other hand, from the perspective of the control bandwidth, the proposed method could expand the gain-cross frequency of $L(j\omega)$ from 848 Hz to 1072 Hz in Fig. 7(b) and decreased the sensitivity by $3 \sim 5$ dB under 1 kHz in Fig. 7(d), in comparison with the conventional method. This result demonstrated the effect of the high-efficiency of the proposed hybrid optimization method for the design problem of a cascade structure FB controller.

V. CONCLUSION

This paper presented a hybrid optimization method that uses SQP and a GA to design a high-performance cascade structure FB controller for a high-order resonant system. The SQP-based optimization could obtain the parameters of a PID compensator that realized a wide bandwidth and satisfied the specified stability margins and sensitivity of the resonant

(a) FB controller $C(j\omega)$

(b) Open-loop $L(j\omega)$

(c) Nyquist diagram of $L(j\omega)$
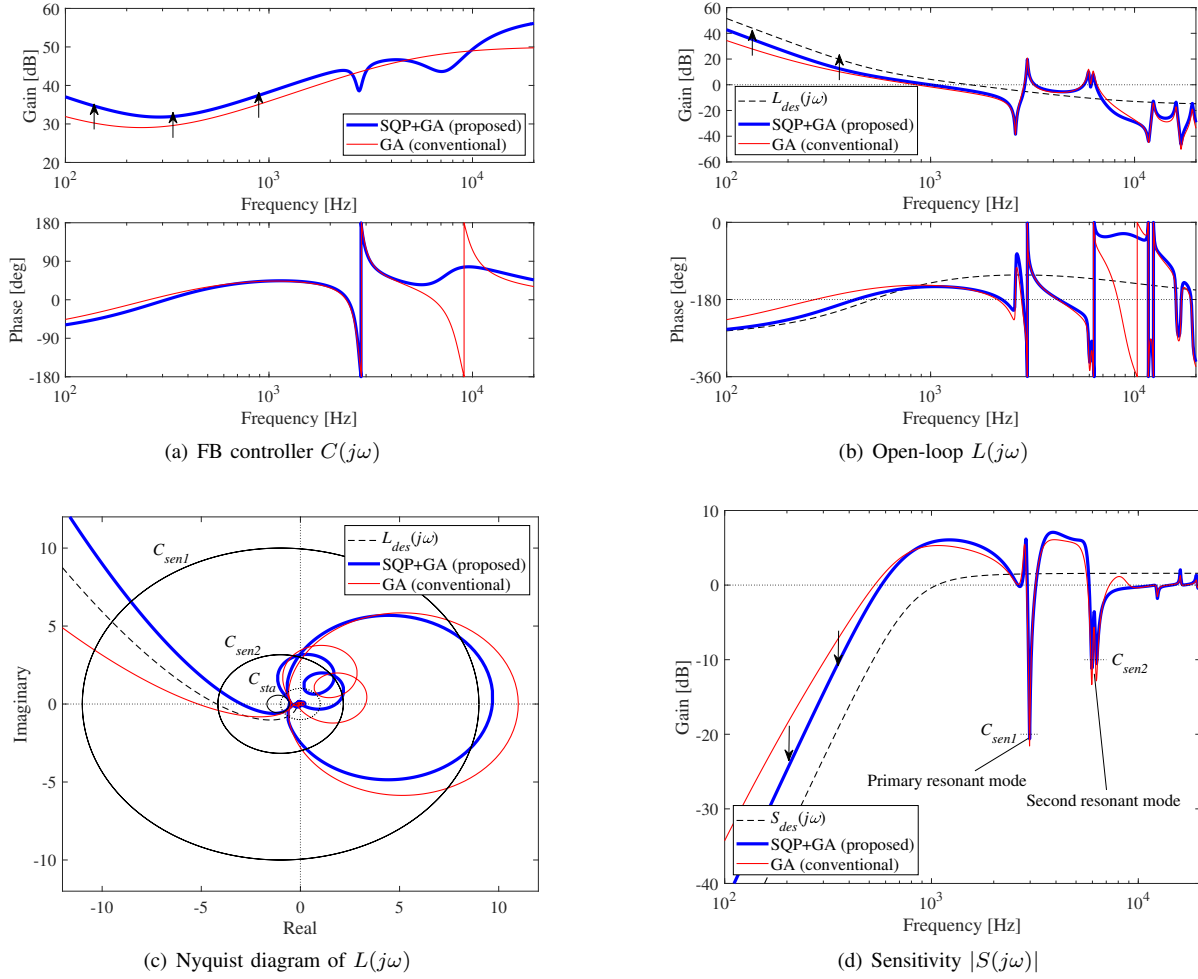
(d) Sensitivity $|S(j\omega)|$

Fig. 7. Frequency characteristics of FB control system: (a) FB controller $C(j\omega)$; (b) open-loop characteristic $L(j\omega)$; (c) Nyquist diagram of $L(j\omega)$; (d) sensitivity characteristic $|S(j\omega)|$.

modes, while the GA-based optimization could obtain the other parameters that could not be found efficiently using the SQP-based optimization. By combing the two optimization methods, the complexity and difficulty of the cascade structure FB controller design problem were effectively reduced. As a result, the control bandwidth was successfully expanded by 26 %(848 rad/s → 1072 rad/s), while shortening the design time by 67 %(3 h → 1 h), compared with those of the conventional GA-based optimization method.

REFERENCES

[1] T. Atsumi, "Emerging technology for head-positioning system in HDDs," *IEEJ J. Ind. Applications*, vol. 5, no. 2, pp. 117–122, 2016.

[2] Y.-Z. Tan and C.-K. Pang, "On using Nyquist plots for relaxing convex conservative approximations in design of robust mechatronic systems," in *Proc. 7th IFAC Symp. Mechatron. Syst.*, Loughborough, UK, pp. 115–119, 2016.

[3] T. Atsumi, T. Arisaka, T. Shimizu, and T. Masuda, "Head-positioning control using resonant modes in hard disk drives," *IEEE/ASME Trans. Mechatron.*, vol. 10, no. 4, pp. 378–384, Aug. 2005.

[4] M. Kanematsu, G. Hilhorst, H. Fujimoto, and G. Pipeleers, "B-Spline parametrized solution of robust PID control using the generalized KYP lemma," in *Proc. 42nd Annu. Conf. IEEE Ind. Electron. Soc.*, Florence, Italy, pp. 5070–5075, 2016.

[5] T. Iwasaki and S. Hara, "Generalized KYP lemma: Unified frequency domain inequalities with design applications," *IEEE Trans. Autom. Control*, vol. 50, no. 1, pp. 41–59, Jan. 2005.

[6] K. Nakamura, K. Yubai, D. Yashiro, and S. Komada, "Fully parameterized controller design method for high control bandwidth using frequency response data sets," in *Proc. 2nd IEEJ Int. Workshop Sensing, Actuation, Motion Control, and Optim.*, Tokyo, Japan, TT1-1, 2016.

[7] H. Khatibi, A. Karimi, and R. Longchamp, "Fixed-order controller design for polytopic systems using LMIs," *IEEE Trans. Automatic Control*, vol. 53, no. 1, pp. 428–434, Jan. 2008.

[8] Y. Maeda and M. Iwasaki, "Circle condition-based feedback controller design for fast and precise positioning," *IEEE Trans. Ind. Electron.*, vol. 61, no. 2, pp. 1113–1122, Feb. 2014.

[9] F. Biral, E. Bertolazzi, and P. Bosetti, "Notes on numerical methods for solving optimal control problems," *IEEJ J. Ind. Applications*, vol. 5, no. 2, pp. 154–166, 2016.

[10] Y. Maeda and M. Iwasaki, "Circle condition-based PID controller design considering robust stability against plant perturbations," in *Proc. 39th Annu. Conf. IEEE Ind. Electron. Soc.*, Vienna, Austria, pp. 6440–6445, 2015.